IEEE Photonics Journal
An IEEE Photonics Society Publication

Open Access

Compact Notch Microwave Photonic Filters Using On-Chip Integrated Microring Resonators

Volume 5, Number 2, April 2013

Jianji Dong
Li Liu
Dingshan Gao
Yuan Yu
Aoling Zheng
Ting Yang
Xinliang Zhang

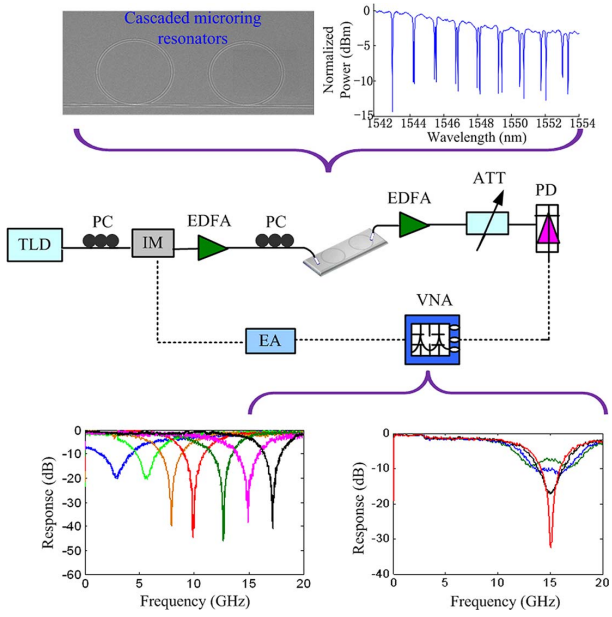

DOI: 10.1109/JPHOT.2013.2245883
1943-0655/$31.00 ©2013 IEEE

IEEE photonics SOCIETY

IEEE

Compact Notch Microwave Photonic Filters Using On-Chip Integrated Microring Resonators

Jianji Dong, Li Liu, Dingshan Gao, Yuan Yu, Aoling Zheng, Ting Yang, and Xinliang Zhang

Wuhan National Laboratory for Optoelectronics, School of Optoelectronic Science and Engineering, Huazhong University of Science and Technology, Wuhan 430074, China

DOI: 10.1109/JPHOT.2013.2245883
1943-0655/$31.00 ©2013 IEEE

Manuscript received December 30, 2012; revised January 30, 2013; accepted February 2, 2013. Date of current version February 26, 2013. This work was supported in part by the National Basic Research Program of China under Grant 2011CB301704, by the Ministry of Education of China through the Program for New Century Excellent Talents under Grant NCET-11-0168, by the Foundation for the Author of National Excellent Doctoral Dissertation of China under Grant 201139, and by the National Natural Science Foundation of China under Grants 60901006 and 11174096. Corresponding author: D. Gao (e-mail: dsgao@mail.hust.edu.cn).

Abstract: We propose and experimentally demonstrate a compact notch microwave photonic filter (MPF) using two integrated microring resonators (MRRs) on a single silicon-on-insulator (SOI) chip. The free spectral ranges (FSRs) of two cascaded MRRs are 160 GHz and 165 GHz, respectively. Due to the vernier effect, the transmission spectrum of cascaded MRRs is a series of bimodal distribution whose interval is an arithmetic sequence. By locating the laser wavelength at the middle of different bimodal intervals and fine tuning it properly, both central frequency and bandwidth of the notch MPF can be tunable. In the experiment, the tunability of central frequency and 3-dB bandwidth are demonstrated from 2.5 GHz to 17.5 GHz and from 6 GHz to 9.5 GHz, respectively. The best rejection ratio of the notch filter is larger than 40 dB. This approach will allow the implementation of low-cost, very compact, and integrated notch MPFs in a silicon chip.

Index Terms: Microwave photonic filter (MPF), microring resonator (MRR), silicon photonics.

1. Introduction

Comparing to conventional microwave filters, microwave photonic filters (MPFs) have attracted increasing interest in the last decade for their advantages, such as huge bandwidth, electromagnetic immunity as well as reconfiguration and tunability [1]. Now, MPFs are used broadly ranging from radar, satellite to wireless communications. In order to process random and unpredictable signals, tunable and reconfigurable MPFs are highly desirable in these systems. To achieve this target, both the central operating frequency and bandwidth of MPFs are required to be tuned [2]. Different optical implementations of MPFs have been proposed [3]–[9]. Among the MPFs, the notch filter can play a critical role in microwave photonic systems to enable the blocking of undesired spectral contents and signal monitoring [10]. Notch MPFs with high quality have been previously demonstrated using differential fiber-delays [11], Bragg gratings [12], and high-birefringence fiber-based optical components [13]–[15]. Compared to these fiber optic systems, silicon-based waveguides can offer distinct advantages of increased stability and reliability, compactness, capability of integration with electronics [10]. In recent years, some MPFs based on silicon microring/disk

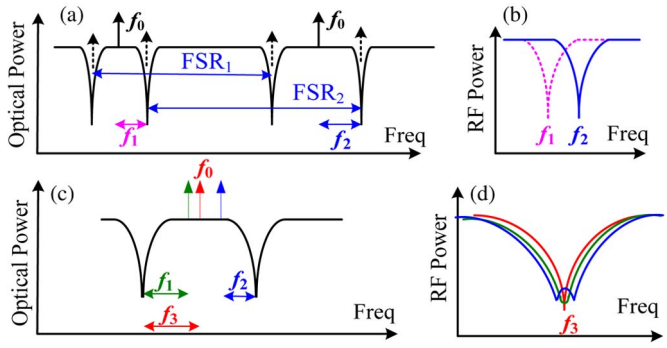

Fig. 1. Tunability of central frequency, where (a) and (b) are optical spectrum of cascaded MRRs and RF spectrum of MPF. Illustration of the tunability of bandwidth, where (c) and (d) are optical spectrum of cascaded MRRs and RF spectrum of MPF.

resonators have been presented, indicating excellent characteristics of reconfigurability [16] or bandwidth tunability [17], but the design and fabrication of the devices are a little complex and difficult. InP-based optical microracetrack notch optical filter was reported [18], which may have potential applications in the notch MPF.

In this paper, we propose and demonstrate a notch MPF based on cascaded microring resonators (MRRs) with different radii. The fabrication is quite simple with only once etching. Due to the vernier effect of the cascaded MRRs spectrum, the central operating frequency and bandwidth of the notch MPF can be easily tuned by changing the laser wavelength. The best rejection ratio of the notch filter is larger than 40 dB. Moreover, because of moving the complexity from the filter to the laser, our scheme offers a simple and integrated solution for low-cost and compact MPFs.

2. Operation Principle

The notch MPF is based on the cascaded MRRs with different free spectral ranges (FSRs, i.e., FSR_1 and FSR_2). The MRR has a single bus waveguide coupled structure, so the transmission spectrum of the through port is a comb notch filter. Due to the vernier effect, the transmission spectrum of cascaded MRRs is a series of bimodal distribution whose interval is an arithmetic sequence. When a random radio frequency (RF) is modulated onto an optical carrier by a Mach–Zehnder modulator (MZM) under small signal modulation, there are an optical carrier (f_0) and both sidebands ($f_0 + f_1$ and $f_0 - f_1$) in the frequency domain. Assume that the optical carrier is located at the middle of a bimodal interval of the MRRs, as shown in Fig. 1(a), then the frequency response of the RF signal reveals a notch filter, as shown in Fig. 1(b). In addition, the notch frequency of RF response is half of the optical bimodal interval. By aligning the optical carrier at the middle of different bimodal intervals, one may tune the notch frequency of RF response. On the other hand, if the optical carrier is slightly shifted from the middle of the bimodal interval, as shown in Fig. 1(c), the bandwidth of the notch MPF can be also tuned according to the frequency offset, as shown in Fig. 1(d). In this way, the bandwidth of the notch MPF can be changed freely while keeping the central frequency constant.

We use a finite-element mode solver (COMSOL Multiphysics) to design the structure of MRR and bus waveguide (WG) and to optimize the performance. In order to reduce the transmission loss of the WG, we design a ridge WG. After optimization, the WG width of both bus WG and bending WG takes about 500 nm. The Si shallow and deep layers have thicknesses of 100 nm and 240 nm, respectively. Fig. 2(a) simulates the effective index of both bus WG and bending WG. One can see that the effective index difference between the WG and MRR is neglectable. Fig. 2(b) calculates the Q value of the transfer spectrum of a single MRR with a radius of 75 μm. One can see that the best coupling gap between the bus WG and bending WG is about 330 nm. In such a case, the simulated effective index and group index of the MRR are 2.82 and 3.98, respectively, when the incident wavelength is 1550 nm. Fig. 2(c) shows the cross section of a ridge MRR on oxide substrate. The

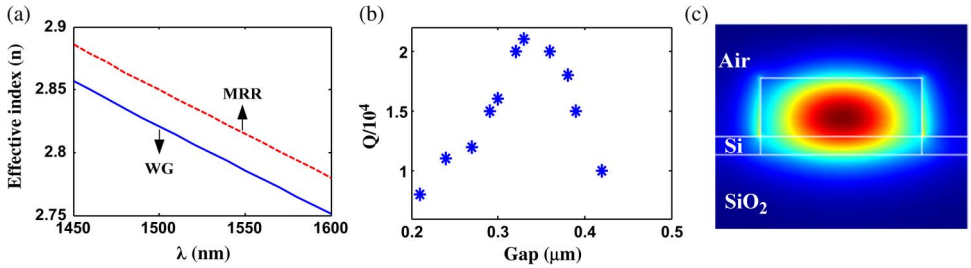

Fig. 2. Simulated results using COMSOL software. (a) Effective index of bus waveguide (WG) and MRR using the designed parameters. (b) Q value of the transfer spectrum for different gaps between the bus WG and MRR. (c) The energy profile of a ridge MRR on oxide substrate.

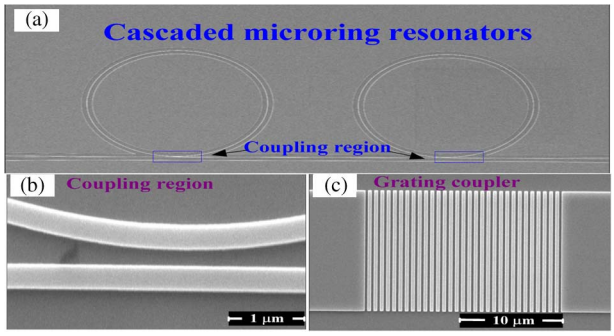

Fig. 3. (a)–(c) SEM images of the cascaded MRRs, coupling region between the bus waveguide and bending waveguide, and the grating coupler, respectively.

energy profile of the fundamental radial TE mode is shown. It is clear that majority of the light-wave energy distributes in the middle of the waveguide.

To experimentally demonstrate the compact notch MPF, we fabricate two cascaded MRRs on the commercial silicon-on-insulator (SOI) wafer. Fig. 3(a) shows the scanning electron microscope (SEM) images of our on-chip cascaded MRRs. The radii of two MRRs are 72.73 μm and 75.0 μm, respectively. The cross section of the MRRs shows a ridge waveguide. The top silicon thickness of the SOI wafer is 340 nm, and the buried oxide layer thickness is 2 μm. The device layout was transferred to ZEP520A photoresist by E-beam lithography (Vistec EBPG5000+ES). Then, the upper silicon layer was etched downward for 240 nm to form a ridge waveguide through induced coupled plasma (ICP) etching (Oxford Instruments Plasmalab System100). The waveguide width of both bus waveguide and bending waveguide is about 500 nm. The coupling gap between the bus waveguide and bending waveguide is about 330 nm. The zoom in coupling region is shown in Fig. 3(b). We employ the vertical grating coupler to couple the optical signal from fiber to silicon waveguide, and the zoom in grating coupler is shown in Fig. 3(c). The grating coupler has a period of 630 nm, and the duty cycle is 56%. The coupling loss of the grating coupler is measured to be 5 dB for a single side.

Fig. 4(a) shows the measured transmission spectrum of the cascaded MRRs using an optical spectrum analyzer (AQ6370B). One can clearly see a series of bimodal distribution whose interval is an arithmetic sequence. The overlapped resonant wavelength for the two MRRs is 1542.98 nm. Beyond this wavelength, the bimodal interval is increased by 5 GHz per FSR period. The FSR of these two MRRs is 160 GHz and 165 GHz, and the 3-dB bandwidth is 0.04 nm and 0.038 nm, respectively. Fig. 4(b) shows a zoom in spectrum, where the bimodal intervals are 25 GHz and 30 GHz, respectively. If the optical carrier is located at the middle of the bimodal interval, the obtained notch MPF has a notch frequency of 12.5 GHz and 15 GHz, respectively.

The frequency response of the notch MPF can also be deduced analytically. Assume that the optical carrier is modulated in an MZM by the RF signal, and the MZM bias is set at the linear region

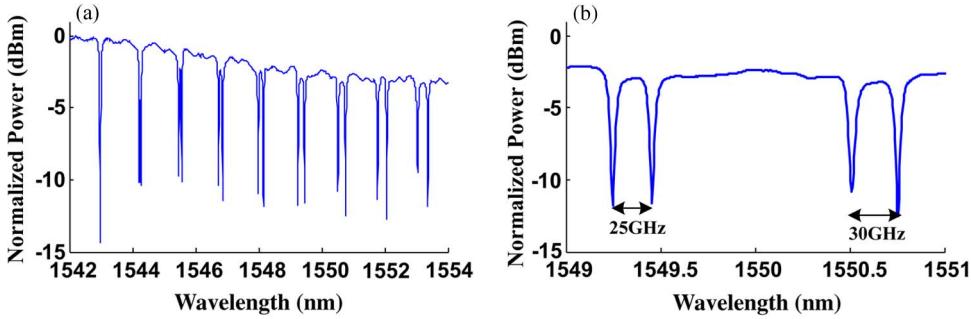

Fig. 4. (a) Measured spectrum of the cascaded MRRs. (b) Zoom in spectrum where the bimodal intervals are 25 GHz and 30 GHz, respectively.

to produce double-sideband modulation. The total voltage offset can be described as

$$V(t) = \frac{1}{2} V_\pi + \alpha V_\pi \cos(\omega_{\mathrm{RF}} t) \tag{1}$$

where V_π is the half-wave voltage, ω_{RF} is the angular frequency of the RF signal, and α is the modulation depth.

In the case of intensity modulation, the output optical field of the MZM can be described by

$$E_{\mathrm{out}}(t) = E_i \cos(\omega_0 t) \cos\left[\frac{\pi}{2V_\pi} \cdot V(t)\right] \tag{2}$$

where E_i is the input optical field, and ω_0 is the angular frequency of the optical carrier.

Then, we substitute (1) into (2) and neglect the high-order sideband, the output optical field of the MZM under a small signal model can be described by

$$E_{\mathrm{out}}(t) = \sqrt{P_0}\left[J_0(m)e^{j\omega_0 t} - J_1(m)e^{j(\omega_0-\omega_{\mathrm{RF}})t} - J_1(m)e^{j(\omega_0+\omega_{\mathrm{RF}})t}\right] \tag{3}$$

where P_0 is the optical power of the source, J_n is the nth-order Bessel function of the first kind, and m is the intensity modulation index. After the signal is transmitted in the cascaded MRRs with a power transmission function of $H(\omega)$, each frequency component will multiply a different frequency weight of $H(\omega)$, so the output optical field can be described as

$$E(\omega) = 2\pi\sqrt{P_0}\left[J_0(m)\sqrt{H(\omega_0)} - J_1(m)\sqrt{H(\omega_0-\omega_{\mathrm{RF}})} - J_1(m)\sqrt{H(\omega_0+\omega_{\mathrm{RF}})}\right]. \tag{4}$$

After detecting of the square-law photodetector (PD) and neglecting the J_1^2 term, we obtain the alternative current (ac) term of the current, which is equal to the product of $\mathrm{E}(\omega)$ and its conjugation

$$i_{ac} \propto 4\pi^2 P_0 J_0(m) J_1(m)\sqrt{H(\omega_0)} \times \left[\sqrt{H(\omega_0-\omega_{\mathrm{RF}})} + \sqrt{H(\omega_0+\omega_{\mathrm{RF}})}\right]. \tag{5}$$

From (5), we can see that if the positive and negative first-order sidebands are aligned at the double notches of the MRRs, respectively, the response of the MPF is a null; otherwise, if both sidebands are far away from the notches, the response is a constant. Therefore, a notch MPF can be obtained. Since the optical carrier is at or near the middle of bimodal intervals, $H(\omega_0)$ is nearly a constant. So the MPF frequency response is mainly determined by the summation of two sidebands' response.

We use the measured spectrum of the cascaded MRRs and substitute it into (5) to calculate the notch MPF response. Fig. 5(a) and (b) shows the notch MPF response when the laser wavelength is located at different bimodal intervals and is just slightly shifted in one bimodal interval, respectively. In order to illustrate the tunability of the central frequency, three different wavelengths at 1546.796, 1548.068, and 1549.352 nm are considered as the optical carriers. In these cases, the bimodal intervals of the MRRs are 15 GHz, 20 GHz, and 25 GHz, respectively. So the notches of

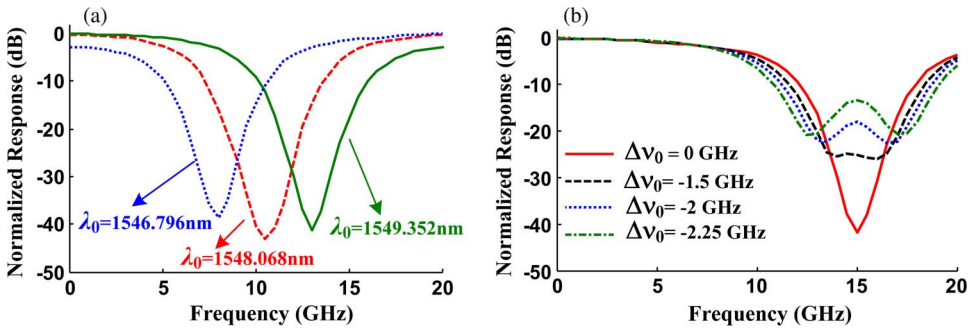

Fig. 5. Simulations of MPF frequency response. (a) Tunable central frequency. (b) Tunable 3-dB bandwidth.

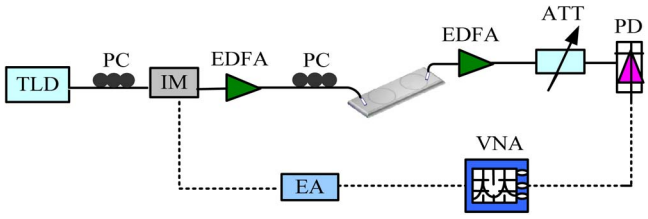

Fig. 6. Experimental setup of the proposed scheme. Solid lines: optical path, dash lines: electrical path, TLD: tunable laser diode, PC: polarization controller, IM: intensity modulator, EDFA: erbium-doped fiber amplifier, ATT: attenuator, PD: photodetector, EA: electrical amplifier, VNA: vector network analyzer.

the MPF are 7.5 GHz, 10 GHz, and 12.5 GHz, as shown in Fig. 5(a). Then, assume that the laser wavelength is located at the middle of bimodal interval of 30 GHz, and the laser wavelength is then shifted by −1.5 GHz, −2.0 GHz, and −2.25 GHz, respectively. Fig. 5(b) shows the simulation of the bandwidth tunability of the notch MPF. It is clear that the bandwidth is varied. Therefore, both central frequency and 3-dB bandwidth $(BW_{3\,dB})$ are tunable in our scheme.

3. Experimental Results

In order to verify the theoretical analysis and the simulation results, we carry out experiments with the configuration, as shown in Fig. 6. A tunable laser diode (TLD) emits a continuous-wave (CW) beam, which has a precisely tuning resolution of 1 pm. The CW beam is modulated by an MZM, which has a modulation bandwidth of 20 GHz. The vector network analyzer (VNA) (Anritsu MS2028C) has a maximum sweeping frequency of 20 GHz. An electrical amplifier (EA) is used to amplify the RF signal from the VNA. A forward erbium-doped fiber amplifier (EDFA) is used to boost the input optical power. A polarization controller (PC) is required since the silicon waveguide operates only in transverse electrical (TE) mode. A backward EDFA is used to compensate the power attenuation by the chip loss. The integrated chip of MRRs is coupled to optical fiber by the vertical grating coupler, which has a 3-dB coupling bandwidth of about 30 nm in *C* band. After amplification by the backward EDFA, the optical signal is converted to electrical signal by the PD and analyzed by the VNA. The PD has a bandwidth of 40 GHz.

Fig. 1 illustrates that, by changing the laser wavelength, we can achieve a notch MPF whose central frequency and bandwidth are variable. Fig. 4(a) proves that the cascaded MRRs have a bimodal distribution due to the vernier effect. Therefore, there should be a mirror distribution in the region shorter than the overlapped resonant wavelength, i.e., the region from 1532 nm to 1542 nm. Then, we select seven laser wavelengths to be aligned at the middle of the bimodal intervals of 5, 10, 15, 20, 25, 30, and 35 GHz, respectively, and the measured notch MPF is shown in Fig. 7(a).

One can see that the notch frequencies are 2.5, 5, 7.5, 10, 12.5, 15, and 17.5 GHz, respectively. Since the spectrum is a series of bimodal distribution whose interval is an arithmetic sequence, the

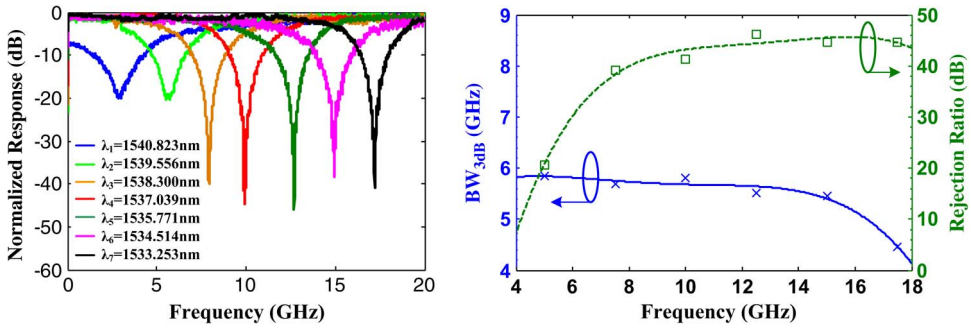

Fig. 7. (a) Measured notch MPFs with tunability of central frequency. (b) Features of 3-dB bandwidth and rejection ratio.

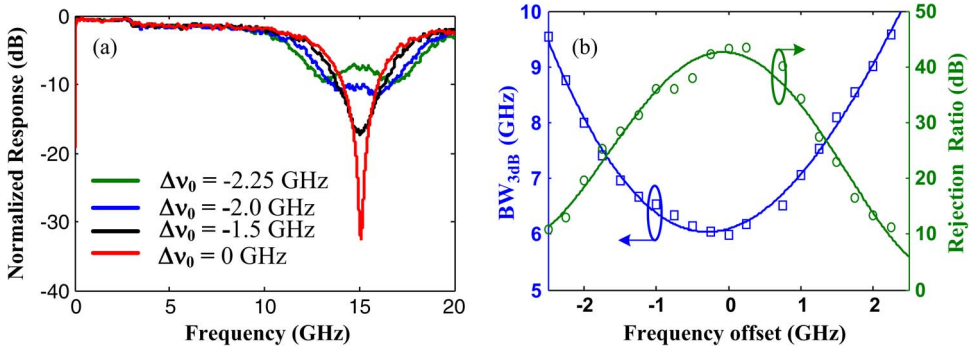

Fig. 8. (a) Measured notch MPFs with tunability of 3-dB bandwidth. (b) Features of 3-dB bandwidth and rejection ratio.

notch frequencies of the notch MPF change as an arithmetic sequence as well. Therefore, the central frequency of the notch MPF is tunable. Fig. 7(b) further demonstrates the 3-dB bandwidth and rejection ratio of the frequency response. As the notch frequency increases, the rejection ratio of the notch MPF increases first and then keeps constant. However, the 3-dB bandwidth decreases. Therefore, the notch MPF has better frequency response at high frequency than at low frequency. This feature can be explained with spectral feature of the cascaded MRRs. In the low-frequency region, the bimodal notches are very close and have strong crosstalk to each other. So the rejection ratio of the notch response is not high at the low frequency.

It should be noted that the FSRs of the two cascaded MRRs can be designed closer. Moreover, it is not difficult to fabricate such MRRs. If the bimodal intervals of two MRRs are designed to be smaller, the central frequency of the notch MPF can be tuned more elaborately. On the other hand, since the 3-dB bandwidth of the two MRRs is around 0.04 nm, the bimodal notches of two MRRs may be overlapped to induce the crosstalk if the bimodal intervals are too close, which can be proved by the experimental results in Fig. 7.

Now, the laser wavelength is located at the middle of bimodal interval of 30 GHz and shifted slightly. The frequency offset to the middle frequency can cause the bandwidth changed. Fig. 8(a) shows the tunable bandwidth of the notch MPF under different frequency offset. When the frequency offsets are set at -1.5 GHz, -2.0 GHz, and -2.25 GHz, one may see the 3-dB bandwidth variation and the rejection ratio variation. In Fig. 8(b), it is clear that as the frequency offset increases, the 3-dB bandwidth also increases from 6 GHz and 9 GHz, while the rejection ratio decreases.

From (5), one can see that RF responses of two sideband components ($\omega_0 - \omega_{RF}$ and $\omega_0 + \omega_{RF}$) could not reach the minimum simultaneously under certain frequency offset. Therefore, the rejection ratio would decrease under the frequency offset. Besides, due to the summation effect of two

misaligned notch frequency responses, the 3-dB bandwidth would increase under the frequency offset. It should be noted that if the frequency offset is appropriate, the frequency response could be a flat band-stop MPF. For example, when the frequency offset is −2 GHz, a flat band-stop MPF is shown in Fig. 8(a).

It should be noted that in our scheme, both central frequency and 3-dB bandwidth are varied by selecting different laser wavelengths. The silicon waveguides including the grating coupler and the ring waveguide are fabricated with ICP etching for only one time. No thermal or electrical nodes are auxiliary, so the silicon processing is quite simple. However, if the notch MPF needs to be precisely manipulated and continuously tuned, then an improved approach is required to enhance the spectral adjustment by fabricating the heater or electrode on the silicon waveguide.

4. Conclusion

A compact notch MPF based on cascaded MRRs has been proposed and experimentally demonstrated. The central operating frequency and 3-dB bandwidth of the MPF can be easily tuned by locating the laser wavelength at the middle of different bimodal intervals and slightly shifting the laser wavelength, respectively. In the experiment, we obtain a high rejection ratio larger than 40 dB, a central frequency tuning range larger than 17 GHz, and a wide tunable bandwidth range from 6 GHz to 9 GHz. Our experiment offers a low-cost and small-size integrated MPF scheme, which can be potentially used to reject certain undesired RF bands in microwave photonic systems.

References

[1] J. Palací, G. E. Villanueva, and J. V. Galán, "Single bandpass photonic microwave filter based on a notch ring resonator," *IEEE Photon. Technol. Lett.*, vol. 22, no. 17, pp. 1276–1278, Sep. 2010.

[2] D. Zhang, X. Feng, and Y. Huang, "Tunable and reconfigurable bandpass microwave photonic filters utilizing integrated optical processor on silicon-on-insulator substrate," *IEEE Photon. Technol. Lett.*, vol. 24, no. 17, pp. 1502–1505, Sep. 2012.

[3] B. Vidal, V. Polo, J. L. Corral, and J. Martí, "Photonic microwave filter with tuning and reconfiguration capabilities using optical switches and dispersive media," *Electron. Lett.*, vol. 39, no. 6, pp. 547–549, Mar. 2003.

[4] B. Vidal, M. A. Piqueras, and J. Martí, "Photonic microwave filter based on spectrum slicing with reconfiguration capability," *Electron. Lett.*, vol. 41, no. 23, pp. 1286–1287, Nov. 2005.

[5] B. Vidal, T. Mengual, C. Ibáñez-López, and J. Martí, "WDM photonic microwave filter with variable cosine windowing based on a DGD module," *IEEE Photon. Technol. Lett.*, vol. 18, no. 21, pp. 2272–2274, Nov. 1, 2006.

[6] B. Vidal, V. Polo, J. L. Corral, and J. Martí, "Harmonic suppressed photonic microwave filter," *J. Lightw. Technol.*, vol. 21, no. 12, pp. 3150–3154, Dec. 2003.

[7] B. Vidal, M. A. Piqueras, and J. Martí, "Tunable and reconfigurable photonic microwave filter based on stimulated Brillouin scattering," *Opt. Lett.*, vol. 32, no. 1, pp. 23–25, Jan. 2007.

[8] X. Yi and R. Minasian, "Microwave photonic filter with single bandpass response," *Electron. Lett.*, vol. 45, no. 7, pp. 362–363, Mar. 2009.

[9] Y. Yu, J. Dong, and E. Xu, "Single passband microwave photonic filter with continuous wideband tunability based on electro-optic phase modulator and Fabry-Pérot semiconductor optical amplifier," *J. Lightw. Technol.*, vol. 29, no. 23, pp. 3542–3550, Dec. 2011.

[10] M. S. Rasras, K.-Y. Tu, and D. M. Gill, "Demonstration of a tunable microwave photonic notch filter using low-loss silicon ring resonators," *J. Lightw. Technol.*, vol. 27, no. 12, pp. 2105–2110, Jun. 2009.

[11] X. Chen, Y. Wu, J. Hodiak, and P. K. L. Yu, "A novel digitally tunable microwave-photonic notch filter using differential group-delay module," *IEEE Photon. Technol. Lett.*, vol. 15, no. 2, pp. 284–286, Feb. 2003.

[12] E. H. W. Chan, K. E. Alameh, and R. A. Minasian, "Photonic bandpass filters with high skirt selectivity and stopband attenuation," *J. Lightw. Technol.*, vol. 20, no. 10, pp. 1962–1967, Nov. 2002.

[13] Y. Yin, X. Che, J. H. Wang, and K. Zheng, "Optical-fiber notch filter for storage ring transverse feedback system," in *Proc. PAC*, 2007, vol. T03, pp. 4075–4077.

[14] E. H. W. Chan and R. A. Minasian, "Coherence-free photonic notch filter," *Electron. Lett.*, vol. 40, no. 21, pp. 1375–1377, Oct. 2004.

[15] W. Zhang, J. A. Williains, and I. Bennion, "Optical fiber delay line filter free of limitation imposed by optical coherence," *Electron. Lett.*, vol. 35, no. 24, pp. 2133–2134, Nov. 1999.

[16] P. Alipour, A. A. Eftekhar, and A. H. Atabaki, "Fully reconfigurable compact RF photonic filters using high-Q silicon microdisk resonators," *Opt. Exp.*, vol. 19, no. 17, pp. 15 899–15 907, Aug. 2011.

[17] L. Chen, N. Sherwood-Droz, and M. Lipson, "Compact bandwidth-tunable microring resonators," *Opt. Lett.*, vol. 32, no. 22, pp. 3361–3363, Nov. 2007.

[18] R. Grover, T. A. Ibrahim, and T. N. Ding, "Laterally coupled InP-based single-mode," *IEEE Photon. Technol. Lett.*, vol. 15, no. 8, pp. 1082–1084, Aug. 2003.